Research on Engineering Structures & Materials
www.jresm.org
MIM Research Group

Research Article

Identification of suspension bridge anchor behavior under service and seismic load conditions using the finite element method

Riyan Wahyu Wibowo [*,1,a], Arief Kusbiantoro [1,b], Samsudin Hamid [2,c], Rifky Rahmad Fauzan [1,d], Faudi Rahmat Riadi [1,e], Kristopal Tambun [1,f], Akbar Khoiru Zad [1,g]

[1]*Department of Civil Engineering, Universitas Negeri Semarang (UNNES), Semarang, Indonesia*
[2]*Department of Civil Engineering, Universiti Teknologi MARA (UITM), Selangor, Malaysia*

Article Info

Article History:

Received 06 Mar 2026

Accepted 15 July 2026

Keywords:

Suspension bridge;
Anchor connection;
Finite element method;
Service load;
Seismic load

Abstract

Suspension bridges are vital infrastructure in an archipelagic country like Indonesia, which demands high structural reliability under complex geographic conditions. This research aims to numerically investigate the structural behavior of anchor connections on pedestrian suspension bridges to ensure their compliance with applicable safety standards. A two-stage comprehensive approach using Finite Element Method (FEM) is applied in this study. The global structural response was modeled using CSi Bridge software, while detailed micro modeling of the anchor joints was developed with ABAQUS/CAE which accommodates material non-linearity and contact interactions between surfaces. Seismic loading is simulated through time history analysis based on the local earthquake response spectrum. The simulation results show that under static and seismic conditions, the anchor connection remains within the elastic limit and meets all safety criteria required. Performance evaluation confirms that all anchor connection components satisfy the demand-capacity ratio requirements. This integrated FEM framework provides a robust methodology for planning and evaluating suspension bridge anchorage system in earthquake-prone regions, to improve structural reliability and safety.

1. Introduction

Suspension bridges are a vital piece of infrastructure that plays an important role in connecting areas with challenging geographical conditions, such as valleys, rivers or straits. Its structural advantages, such as the ability to span long spans with efficient use of materials and high aesthetic value, make it a popular choice in the construction of transportation infrastructure, including pedestrian bridges [1,2]. However, the flexible nature of suspension bridge structural systems also makes them vulnerable to dynamic loads, including earthquake loads, which have the potential to threaten the safety and reliability of the structure [3,4]. This vulnerability is exacerbated by Indonesia's location in an active seismic zone, with the potential for high-magnitude earthquakes due to complex tectonic plate interactions.

One of the critical components in a suspension bridge system is the anchor connection, which functions as a link between the steel pylon and concrete pylon in a composite pylon system. This connection plays an important role in transmitting forces from service loads (such as dead load, live load, and wind) as well as seismic loads between pylon sections with different materials [5,6]. In the context of steel structures, column base connections have long been identified as critical

*Corresponding author: riyanwahyu@students.unnes.ac.id
[a]orcid.org/0009-0006-1715-8906; [b]orcid.org/0009-0005-1693-5219; [c]orcid.org/0000-0003-2831-4880; [d]orcid.org/0009-0002-1713-581X; [e]orcid.org/0009-0006-5377-8889; [f]orcid.org/0009-0008-8473-0479; [g]orcid.org/0009-0006-1758-9001
DOI: http://dx.doi.org/10.17515/resm2026-1549st0306rs

components whose behavior significantly influences the performance of the entire system [7,8]. Failure of anchor connections can compromise the structural integrity of the pylon and potentially affect the overall stability of the bridge [9,10]. Therefore, an in-depth understanding of the behavior of anchor connections under various loading conditions is very important, especially in designing earthquake-resistant and reliable structures [11].

Previous research has developed various analytical methods to evaluate the performance of bridge structures, including the use of the Finite Element Method (FEM). FEM enables accurate numerical modeling to analyze structural responses under static and dynamic loading conditions, including the simulation of non-linear behavior of materials and interactions between components [12,13]. To study the behavior of these complex connections, finite element modeling (FEM) has been proven to be able to represent the actual conditions of the structure with high accuracy [14,15]. A well-calibrated FEM model allows accurate simulation of structural response under various loading scenarios, including dynamic and seismic analysis of critical components [16-20]. However, studies that specifically integrate macro and micro modeling to analyze the behavior of anchor connections in pedestrian suspension bridges under combined service and seismic loads are still limited [21,22]. The gap in this research lies in the limited nature of holistic analysis, especially one that simultaneously considers the interaction between the global behavior of bridge structures and local responses at critical connections [23,24]. In addition, evaluation of the performance of anchor connections under various realistic earthquake scenarios, especially those that represent the seismic characteristics of the local area, has not yet been studied comprehensively in the literature.

Recent studies of column base connections emphasize the advantages of extended anchor configurations in improving seismic performance. Experimental evidence shows that anchor bolts with a minimum tension length of four times their diameter produce more ductile connections and are able to absorb earthquake energy more effectively [25,26]. In addition, field observations following large earthquakes such as the 2010 Maule Earthquake in Chile inform the superior performance of connections with well-planned details, where connections with adequate strain lengths show exceptional resistance to cyclic loads [27,28]. To achieve optimal design, standards such as AISC 341-16 and ACI 318-19 provide a framework and practical recommendations, including the ratio of free length to bolt diameter to guarantee performance [7,29,30]. Extensive validation of FEM modeling has also demonstrated its effective capability in predicting the cyclic response of joints, including hysteresis patterns, rotational capacities, and failure mechanisms [31,32]. The selection of the pedestrian suspension bridge in Bogor Regency as a research object was based on three main considerations. First, the topography of Bogor Regency, which is hilly and has river valleys, makes suspension bridges the most economical and structurally efficient solution compared to beam or arch bridges, which require large foundations or expensive intermediate pillars. Second, this bridge functions as an important link between two densely populated residential areas separated by a steep ravine, with around 500 people crossing every day, including school children and local farmers. Third, Bogor Regency is classified as a high earthquake risk zone (PGA 0,4913g), so evaluating the seismic performance of suspension bridge anchor connections at this location provides valuable insight into infrastructure in areas with similar geological conditions throughout the Indonesian archipelago.

Based on this background, this research aims to identify the behavior of anchor connections on pedestrian suspension bridges under the influence of service loads and seismic loads using the Finite Element Method (FEM) approach. This study integrates macro modeling of the bridge structure as a whole using CSi Bridge v25 software with detailed micro modeling of anchor connections using ABAQUS/CAE. The research location is the pedestrian suspension bridge in Bogor Regency, West Java, located at coordinates 6°42' S latitude and 106°52' E longitude, which is in an active seismic zone. The analysis method used includes a detailed evaluation of the anchor connection design parameters under service and seismic loading conditions, including time history analysis using earthquake recordings that correspond to local seismic characteristics [33].

With this comprehensive approach, the results of this research are expected to not only identify the force transfer mechanisms and stress distribution patterns in anchor connections [34], but also evaluate their performance based on parameters such as displacement, stress, and strain. It is hoped that the results of this research can provide design recommendations that increase the reliability and safety of anchor connections on suspension bridges in seismic areas, as well as contribute to the development of planning guidelines that are more adaptive to the characteristics of earthquakes in Indonesia. Apart from that, this study is also expected to enrich civil engineering literature regarding the application of FEM in the analysis of the structural behavior of suspension bridges under extreme loading conditions, as well as becoming a reference for the development of more robust design standards in the future.

This study contributes to the existing literature in several significant ways. First, it presents an integrated macro-micro finite element modeling approach for pedestrian suspension bridge anchor connections, combining global structural analysis (CSi Bridge) with detailed local modeling (ABAQUS/CAE). This integration allows for a comprehensive understanding of anchor behavior, from overall structural response to local stress and strain distributions. Second, it evaluates anchor performance under both static service loads and seismic time history analysis using site-specific earthquake parameters for an active seismic zone in Indonesia, providing insights into the seismic vulnerability of critical bridge components that are often overlooked in macro-scale analysis. Third, it offers comprehensive design verification based on SNI 1729:2020 and AISC 360-16, including tensile, shear, combined tension-shear, and anchorage length checks, with demand-capacity ratios (DCRs) calculated for each critical component. Fourth, it provides practical recommendations for future research, including experimental validation, advanced constitutive modeling (kinematic hardening), and soil-structure interaction (SSI) analysis, which can guide engineers and researchers in designing more reliable suspension bridge anchor system in earthquake-prone regions. The findings of this study are expected to serve as a valuable reference for both researchers and practitioners in the field of bridge engineering, particularly in developing countries with similar seismic characteristics.

The remainder of this paper is organized as follows. Section 2 presents the finite element modeling methodology, including the macro-modeling of the suspension bridge in CSi Bridge v25 and the micro-modeling of the anchor connection in ABAQUS/CAE V6.14, as well as the material parameters, seismic load definitions, and boundary conditions. Section 3 presents the numerical results from static and dynamic analyses, including stress, strain, and deformation distributions, followed by design verification and demand-capacity ratio (DCR) calculations based on SNI 1729:2020 and AISC 360-16. Section 4 provides the conclusions and recommendations for future research, including experimental validation, advanced constitutive modeling, and soil-structure interaction analysis.

2. Finite Element Modeling

This research uses an integrated hierarchical modeling approach to bridge the macro and micro scales in analyzing the behavior of suspension bridge anchor connections. Overall structural modeling was carried out with CSi Bridge v25, while detailed analysis of anchor connections was developed using ABAQUS/CAE V6.14 by considering material non-linearity and contact interactions between components. All modeling stages refer to Detail Engineering Design (DED) data for the Pedestrian Suspension Bridge located in Bogor Regency, West Java. The research object is situated at GPS coordinates 6°42' S, 106°52' E, as indicated in the location map (Fig. 1) below.

Fig. 1. Research location map

2.1 Model Geometry and Structural Configuration

The object of the research is a Pedestrian Suspension Bridge with a main span of 275 m, a width varying between 6-12 m, and a pylon height of 54,65 m. This structure is a class I suspension bridge with an innovative triple-layered transparent glass floor (laminated tempered glass) of 30 mm thick combined with a Wood Plastic Composite (WPC) floor. The structural configuration consists of a main cable in the form of a 2 x 14 Ø52 mm wire rope with a minimum tensile strength (fu) of 1.770 MPa and a yield strength (fy) of 1.062 MPa, a hanging cable in the form of a 2 x 1 Ø40 mm steel rod with fy = 460 MPa and fu = 550 MPa, a main girder in the form of a 1.500 x 600 mm steel box girder with a plate thickness of 25 mm, and a transverse girder in the form of a 500 x 500 mm box beam with a plate thickness of 25 mm. The bridge pylon is a combination of reinforced concrete with a quality of f'c = 30 MPa and a hollow steel profile (BJ41) with fy = 250 MPa and fu = 410 MPa. The anchor block is made of reinforced concrete f'c = 30 MPa with dimensions of 9.000 x 5.250 x 5.000 mm. The anchor system uses 68 ASTM A325M anchor bolts with a diameter of 36 mm and a length of 1.200 mm, with fy = 660 MPa and fu = 830 MPa, and a base plate in the form of a structural steel plate measuring 2.500 x 5.500 mm and a thickness of 80 mm with fy = 250 MPa and fu = 410 MPa.

2.2 Macro Modeling with CSi Bridge v25

The overall bridge structure modeling was performed using CSi Bridge v25 with a 3D finite element approach. Frame elements were used to model the main girder, transverse girder, pylon, main cable, and suspension cable. The boundary conditions at the foundation and anchor blocks were modeled as fully fixed supports. The overall suspension bridge structure modeling can be seen in (Fig. 2).

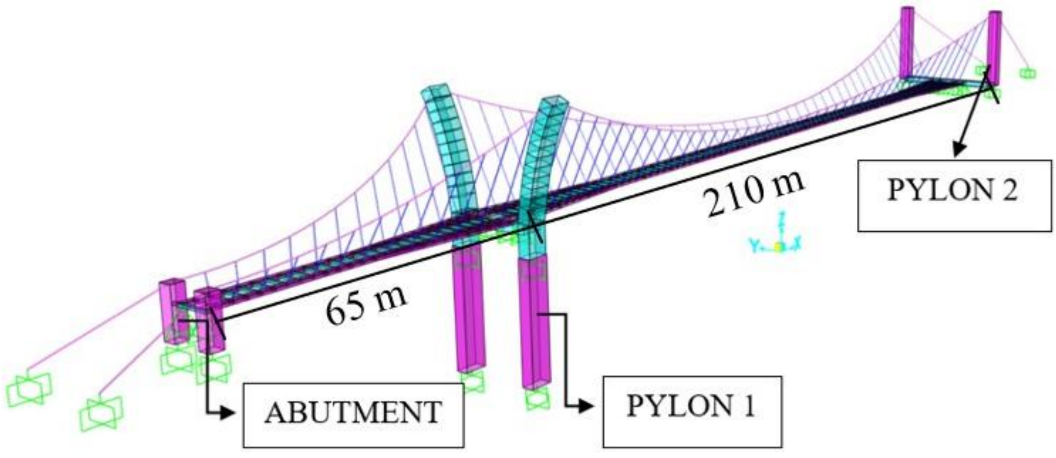

Fig. 2. Pedestrian suspension bridge

The loads applied in macro modeling include dead loads calculated automatically based on the self-weight of all structural components, as well as additional dead loads in the form of railing loads of 0,085 kN/m on each longitudinal girder. The live load used is a uniform load of 5 kPa on the entire bridge floor area in accordance with SE Menteri PU No. 2 Tahun 2010 (Guidelines for Technical Planning of Pedestrian Suspension Bridges). In addition, a wind load of 1,3 kN/m^2 is applied based on the same regulation, acting on the side plane (longitudinal vertical plane) of the structure, which is considered as a lateral load in the analysis.

2.2.1 CSi Bridge Analysis Results

The macro-modeling analysis in CSi Bridge v25 provided the global structural response of the suspension bridge under both static and seismic loading conditions. Figure 3 presents key results from the CSi Bridge analysis, including the internal force distributions. These global results were used to determine the reaction forces at the anchor connection (Pu, Mu, Vu), which were then applied as boundary conditions in the detailed micro-modeling in ABAQUS/CAE (see Section 2.3.2).

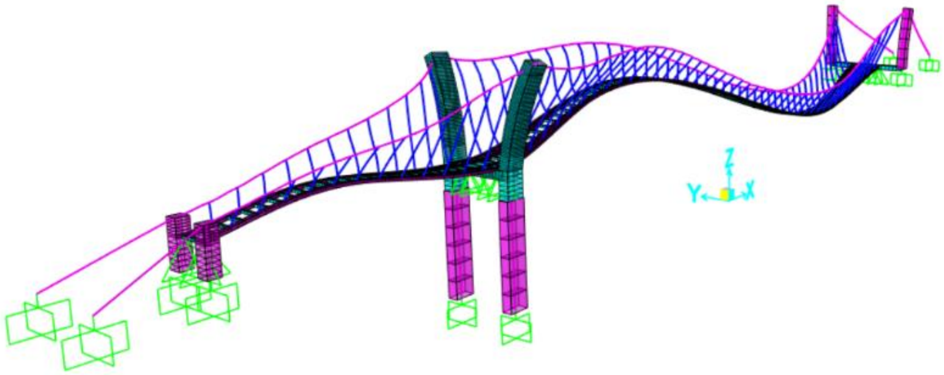

(a)

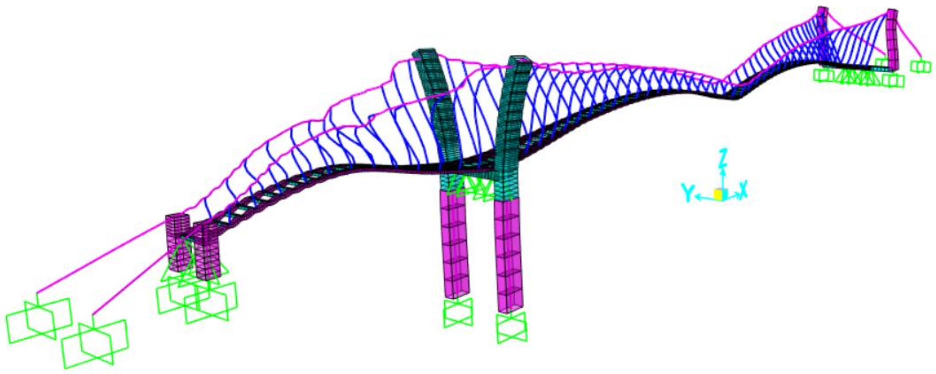

(b)

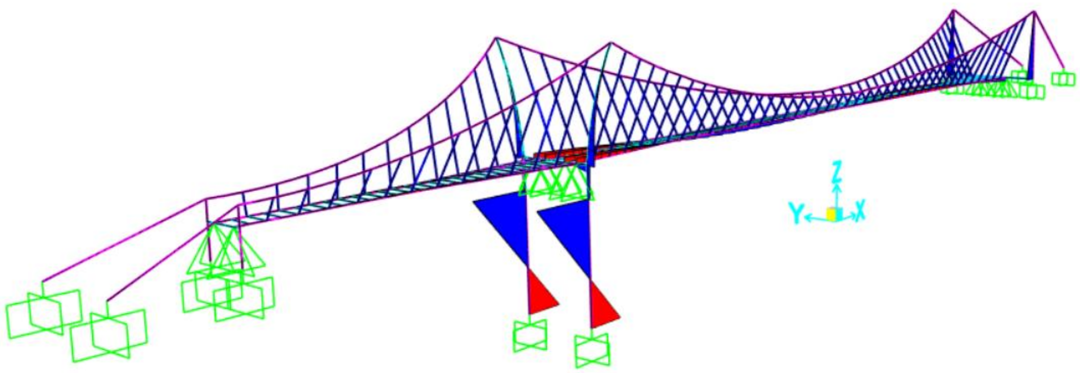

(c)

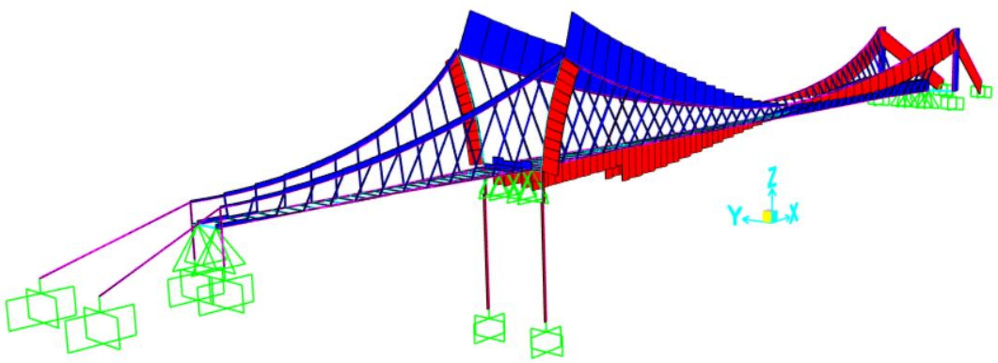

(d)

Fig. 3. Global structural responses from CSi Bridge v25: (a) deformed shape under static loading; (b) deformed shape under seismic loading; (c) bending moment diagram of the suspension bridge; (d) axial force distribution in the main cable

2.3 Micro Modeling with ABAQUS/CAE V6.14

The detailed modeling of the anchor connection was developed using ABAQUS/CAE V6.14 with a higher level of element discretization. The modeled components include anchor bolts and pedestal concrete. The entire geometry is modeled as a 3D continuous body with a global coordinate system where the X and Z axes represent the horizontal direction, while the Y axis represents the vertical direction. All analyses in ABAQUS/CAE V6.14 were performed using double precision arithmetic. Double precision was selected to ensure numerical accuracy and stability, particularly for the nonlinear contact interactions and the seismic time history analysis, where large numbers of increments are required. The use of double precision minimizes round-off errors and provides more accurate stress and strain predictions, especially in regions of high stress concentration around the anchor bolts.

2.3.1 Element Types and Mesh Convergence

The concrete components are modeled using eight-node three-dimensional solid elements with three translational degrees of freedom at each node in the global X, Y, and Z directions. The C3D8R type of reduced integration solid element was chosen to improve computational efficiency while minimizing the potential for shear locking, which is common in reinforced concrete structural modeling. The anchor bolts are also modeled using the same eight-node solid elements (C3D8R) to accurately represent the three-dimensional stress distribution and interaction with the surrounding concrete.

The interaction between concrete and embedded anchor bolts is simulated using the embedded region technique with the assumption of a perfect bond, so that strain compatibility between the two materials is guaranteed during the loading process. The surface contact interaction between the anchor bolt and concrete is defined with a friction coefficient of 0,3 using the surface-to-surface contact algorithm. The friction coefficient of 0,3 was adopted for the tangential behavior of the surface-to-surface contact between the anchor bolt and the concrete pedestal. This value was selected based on established practices in finite element modeling of steel-concrete interface and international design standards. According to prEN 1993-1-8:2023 (Eurocode for the design of steel joints), a friction coefficient of 0,3 is specified for base plate and grout layer interfaces under conditions where steel failure governs. Additionally, numerous numerical modeling studies, such as those conducted in ABAQUS for similar steel-concrete interactions, routinely adopt a friction coefficient of 0,3 as a realistic and conservative value. This value provides a representative basis for simulating the frictional load transfer mechanism under both static and seismic loading conditions.

A mesh size of 500 mm was applied to all concrete elements, while the anchor bolt elements were discretized with a very small mesh size of 5 mm. Mesh convergence tests were performed by varying the element size from 5 mm to 500 mm to ensure that the simulation results were insensitive to discretization changes. With this configuration, the anchor connection model consisted of 18.762 elements and 23.019 nodes. A summary of the element types and numbers is presented in Table 1.

Table 1. Type and number of elements in a finite element model

Component	Element Type	Element Shape	Geometric Order	Number of Elements	Number of Nodes
Pedestal concrete	C3D8R	Hexahedral	Linear	96	175
Anchor bolt	C3D8R	Hexahedral	Linear	18.762	23.019

2.3.1.1 Mesh Refinement Strategy in Critical Regions

To accurately capture stress concentrations around the anchor bolts and at the steel-concrete interface, a graded mesh refinement strategy was employed in ABAQUS/CAE. The element discretization was designed to balance computational efficiency with solution accuracy, particularly in regions where high stress gradients are expected.

Three mesh zones were defined based on the distance from the anchor bolt surface:

- Fine mesh zone (5 mm element size): This zone includes the anchor bolt shank and threaded region, as well as the concrete volume immediately surrounding the bolt within a radius of 50 mm from the bolt surface. This high-resolution mesh ensures accurate resolution of high stress gradients that typically develop at the steel-concrete interface due to bearing and friction. The 5 mm element size was determined through a mesh convergence study, where element sizes were varied from 5mm to 500 mm. Further refinement beyond 5 mm produced less than 1% change in peak stress values, confirming that the solution had converged.
- Transition mesh zone (10-20 mm element size): This zone covers the concrete region extending from 50 mm to 200 mm from the bolt surface. This zone provides a gradual transition between the fine mesh around the bolt and the coarse mesh in the far field, preventing abrupt changes in element size that could introduce numerical errors such as stress discontinuities at element boundaries.
- Coarse mesh zone (500 mm element size): This zone covers the remaining concrete volume distant from the anchor bolt (beyond 200 mm from the bolt surface), where stress gradients are relatively low. The coarse mesh reduces the total number of elements (18.762 elements as reported in Table 1) and improves computational efficiency without sacrificing solution accuracy.

Mesh quality was verified by checking element aspect ratios and Jacobian values. All elements had aspect ratios below 5:1 and Jacobian values above 0,6, indicating good mesh quality suitable for nonlinear element analysis. The graded mesh refinement strategy ensures that stress concentrations around the anchor bolts and at the embedded interface are accurately captured, which is critical for the stress predictions presented in Section 3.

2.3.1.2 Reduced Integration and Hourglass Control

The C3D8R element is an 8-node linear brick element with reduced integration, employing a single integration point at the element centroid rather than the standard 8 integration points (2 x 2 x 2 Gauss quadrature) used in fully integrated elements. This element type was selected for two primary reasons: (1) to avoid shear locking, which commonly occurs in fully integrated elements under bending-dominated deformation, and (2) to improve computational efficiency by reducing the number of integration points per element. However, reduced integration elements are susceptible to hourglass modes (zero-energy deformation patterns) that can produce spurious results if not properly controlled. To mitigate this issue, the enhanced hourglass control algorithm available in ABAQUS/CAE was activated. This algorithm applies artificial stiffness to resist hourglass deformation without significantly affecting the physical response of the model.

The quality of the solution was verified by monitoring the artificial strain energy (ALLAE) and comparing it to the total internal energy (ALLIE) throughout all simulations. In finite element analysis, hourglass effects are generally considered negligible if the ratio ALLAE/ALLIE remains below 5-10%. In the present analysis:

- Under static loading : ALLAE/ALLIE < 3%
- Under seismic (dynamic) loading : ALLAE/ALLIE < 5%

These values confirm that hourglass effects were negligible and did not compromise the accuracy of the stress, strain, of deformation predictions presented in Section 3. Therefore, the use of C3D8R elements with enhanced hourglass control is justified for this study.

2.3.2 Boundary Condition and Loading Procedure

Boundary conditions are applied to realistically represent the experimental configuration and structural assumptions. On the bottom surface of the pedestal concrete, all translational degrees of freedom are restrained to simulate the fixed support condition. The load combinations used in this analysis refer to SNI 1729:2020 and AISC 360-16 (LRFD method). A total of five load combinations were evaluated in CSi Bridge v25, as summarized in Table 2.

Table 2. LRFD load combinations (SNI 1729:2020 & AISC 360-16)

No.	Load Combination
1	1,4D
2	1,2D + 1,6L + 0,5 W
3	1,2D + 1,6L + 0,5W + 0,5E
4	1,2D + 1,0L + 1,0E
5	0,9D + 1,0E

Where; D= Dead load (self-weight of structural components), L= Live load (pedestrian load 5 kPa), W= Wind load (1,3 kN/m^2), E= Earthquake load (time history analysis based on local response spectrum).

From these five load combinations, the maximum value of each reaction component at the anchor connection was selected for design purposes, as follows:

- Pu (max) = 17.329 kN
- Mu (max) = 9.667 kNm
- Vu (max) = -7.675,7 kN

These maximum values were subsequently applied as boundary conditions on the top surface of the anchor bolt using kinematic coupling. The loading procedure was carried out in two sequential stages. In the first stage, a compressive axial load was applied to the top surface of the anchor bolt and maintained constant throughout the analysis. In the second stage, a lateral load was applied through displacement control on the side surface of the anchor bolt with an amplitude corresponding to the recorded earthquake time history. This loading scheme was designed to simulate the response of the anchor connection under combined axial and lateral loads, thus allowing a non-linear evaluation of the anchor behavior under service and seismic load conditions. The detailed geometry and boundary conditions of the anchor connection model are presented in (Fig. 4).

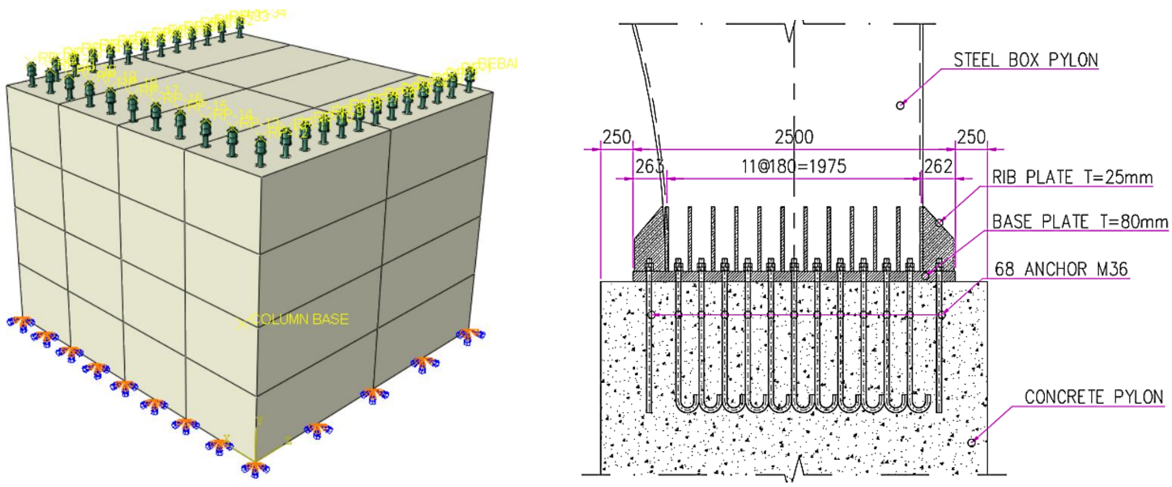

(a) (b)

Fig. 4. Geometric details and boundary conditions of the anchor connection model: (a) Isometric; (b) Longitudinal section

2.3.2.1 Boundary Condition Simplification and Soil-Structure Interaction

In the current model, the bottom surface of the pedestal concrete was modeled as fully fixed (encastre), meaning all translational degrees of freedom (U1, U2, U3) were restrained. This simplification assumes that the foundation and underlying soil provide infinite stiffness, which may not fully represent actual field conditions. In reality, foundation flexibility and soil-structure interaction (SSI) can influence the structural response, particularly for bridges located on soft soil deposits or subjected to seismic loading.

- Justification for this simplification: The fully fixed assumption was considered acceptable for the present analysis because the primary focus was the local behavior of the anchor connection under load combinations that produce maximum forces at the connection. Additionally, the fully fixed assumption represents a conservative upper bound for anchor connection force demands, as foundation flexibility would typically reduce the forces transferred to the anchor by allowing some energy dissipation through soil deformation.
- Limitations acknowledged: This simplification does not capture: (1) foundation settlement or rotation under moment loading, (2) energy dissipation through soil damping, (3) potential changes in natural frequencies due to SSI, or (4) nonlinear soil behavior under cyclic seismic loading.
- Recommendation for future research: For future studies, particularly for bridges located on soft soil or when displacement-sensitive seismic analyses are required, it is recommended to incorporate soil-structure interaction using either spring elements (e.g., Winkler foundation model with soil stiffness derived from SPT-N values as presented in Section 2.5.1) or continuum soil elements to capture foundation flexibility and energy dissipation through the soil medium.

2.4 Material Parameters of the Model

A numerical model was developed based on material parameters and modeling strategies that have been widely adopted in previous numerical studies of steel and concrete structural connections. The reliability of the adopted approach was evaluated by the model's ability to consistently reproduce the response characteristics of the anchor connection according to the behavioral mechanisms reported in the literature.

2.4.1 Concrete Material Model

Modeling the behavior of concrete as a non-homogeneous and anisotropic material is one of the main challenges in finite element analysis of reinforced concrete structures. Among various non-linear concrete constitutive models available in ABAQUS such as smeared cracking model and brittle cracking model, the Concrete Damage Plasticity (CDP) model is adopted in this study due to its comprehensive and integrated formulation [35,36]. The CDP model incorporates the fundamental components of classical plasticity theory, including yield criterion, flow rule, and hardening rule, which are effectively used to simulate the non-linear behavior of concrete under combined stress conditions.

The concrete material parameters considered in the numerical analysis include density, initial modulus of elasticity (E_0), Poisson's ratio (ν), and concrete compressive and tensile strengths. The concrete Poisson's ratio is assumed to be constant at 0,2. In addition, the numerical modeling uses the Concrete Damage Plasticity (CDP) parameter, the values of which are summarized in Table 3.

Table 3. Input parameters concrete damage plasticity

Plasticity Parameters	Notation	Value
Dilatation angle	ψ	31°
Shape factor	Kc	0,667
Stress ratio	fb0/fc0	1,16
Eccentricity	ε	0,1

2.4.2 Steel Material Model

The uniaxial stress-strain behavior of the anchor bolts is modeled assuming a perfect elastoplastic response, with an elastic modulus of E = 200.000 MPa and a Poisson's ratio of ν = 0,3. The plastic state of the steel is represented by defining the yield stress and the corresponding plastic strain. This plastic behavior is modeled using a bilinear stress-strain relationship, which is commonly adopted to represent the inelastic response of reinforcing steel in nonlinear finite element analysis. The material parameters of the steel used for the anchor connection components are summarized in Table 4. These dimensions and material properties were used as input for the design verification (demand-capacity ratio) presented in Section 3.3.

Table 4. Stress-strain properties of steel materials

Component	Diameter (mm)	Length (mm)	Yield Stress fy (MPa)	Yield Strain εy	Ultimate Strength fu (MPa)	Ultimate Strain εu
Anchor bolt (ASTM A325M)	36	1.200	660	0,0033	830	0,15

2.5 Seismic Load Parameters

2.5.1. Site Classification and Soil Properties

A geotechnical investigation was carried out at the bridge site to determine the soil profile and site class. Standard Penetration Test (SPT) was performed at several borehole locations. Based on SPT results, the average SPT-N value for the top 30 meters of the soil profile was N = 19. According to SNI 1726:2019 (Table 9), a site with an average SPT-N value between 15 and 50 is classified as medium soil (site class SD). Therefore, the bridge site was classified as medium soil (SD).

2.5.2 Design Response Spectrum and Design Code

The design response spectrum used in this analysis was developed based on SNI 1726:2019 (Earthquake resistance design procedures for buildings and non-building structures), which adopts the provisions of AISCE/SEI 7-16 with modifications tailored to Indonesian seismic conditions. The seismic parameters (peak ground acceleration, spectral accelerations, and amplification factors) were obtained from the Peta Gempa Indonesia 2017 (Indonesian Earthquake Map 2017) using the online application "Desain Spektra Indonesia" developed by the Directorate General of Human Settlements, Ministry of Public Works and Housing (PU Cipta Karya), accessible at https://rsa.ciptakarya.pu.go.id/.

For Bogor Regency location, based on a 7% probability of exceedance in 75 years (return period of approximately 1.000 years) and a medium soil site class (SD), the following seismic parameters were obtained: PGA = 0,4913g, Ss = 1,0580g, S1 = 0,4815g, Fa = 1,0768, Fv = 1,5185, SDS = 1,1392g, and SD1 = 0,7311g.

Based on the medium soil site class (SD), the site amplification factor is interpolated to obtain an acceleration-related vibration amplification factor (FPGA) of 1,0087, a short-period amplification factor (Fa) of 1,0768, and a 1-second period amplification factor (Fv) of 1,5185. From these amplification factor values, the soil surface spectra values are calculated to obtain A_s of 0,4956g, SDS of 1,1392g, and SD1 of 0,7311g, with characteristic spectrum periods of T_s = 0,6417 seconds and T_0 = 0,1283 seconds. This design response spectrum was then used as a basis for time history analysis applied to the bridge macro-structure modeling in CSi Bridge v25.

2.5.3 Damping Assumptions for Time History Analysis

For the time history analysis conducted in CSi Bridge v25, Rayleigh damping was assumed to represent energy dissipation in the bridge structure. Rayleigh damping assumes that the damping matrix [C] is proportional to a linear combination of the mass matrix [M] and the stiffness matrix [K], expressed as:

$$[C] = \propto [M] + \beta\,[K] \tag{1}$$

Where α is the mass-proportional damping coefficient and β is the stiffness-proportional damping coefficient.

According to SNI 2833:2016 (Standard for planning of bridge resistance to earthquake loads), a damping ratio of 5% of critical damping (ξ = 0,05) is recommended for the first two vibration modes of bridge structures. This value is appropriate for a pedestrian suspension bridge with a steel-concrete hybrid pylon system as modeled in this study. The Rayleigh damping coefficients (α and β) were calculated based on the first two natural frequencies of the bridge model using the following equations:

$$\propto = \frac{4\pi f_1 f_2 \xi}{f_1 + f_2}, \qquad \beta = \frac{2\xi}{\pi(f_1 + f_2)} \tag{2}$$

Where; ξ= 0,05 (damping ratio), f_1= first natural frequency (Hz), f_2= second natural frequency (Hz)

Based on the modal analysis result from CSi Bridge v25, the first natural frequency was determined as f1 = 0,32655 Hz and the second natural frequency as f2 = 0,40742 Hz. Substituting these values into the Rayleigh damping equations yields a mass-proportional damping coefficient $\propto = 0{,}1138$ and a stiffness-proportional damping coefficient $\beta = 0{,}0434$. Energy dissipation behavior: Because the anchor connection remained elastic throughout the seismic analysis (maximum stress from FEM analysis = 303,44 MPa < yield stress = 660 MPa), as demonstrated in Section 3.3.3, energy dissipation occurred primarily through material damping within the elastic range rather than through hysteretic behavior. No inelastic cyclic degradation or energy dissipation through plastic hinging was observed in the anchor connection under the design-level seismic event considered in this study. This elastic response is consistent with the design objective of keeping the anchor connection within safe limits (DCR < 1.0) under design-level seismic events. For future studies involving larger seismic demands that may induce yielding in the anchor bolts, it is recommended to adopt a hysteretic damping model or to explicitly model cyclic plasticity (e.g., using a kinematic hardening material model) to accurately capture energy dissipation through plastic deformation under repeated cyclic loading.

2.5.4 Seismic Input and Response Spectrum

The seismic input for the time history analysis was obtained from the design response spectrum developed for the Bogor Regency location. The response spectrum curve was generated using the online application "Desain Spektra Indonesia", developed by the Directorate General of Human Settlements, Ministry of Public Works and Housing (PU Cipta Karya), accessible at https://rsa.ciptakarya.pu.go.id/. This application is based on the Indonesian Earthquake Map 2017 and SNI 1726:2019, and provides spectral acceleration values for specific locations and site classes.

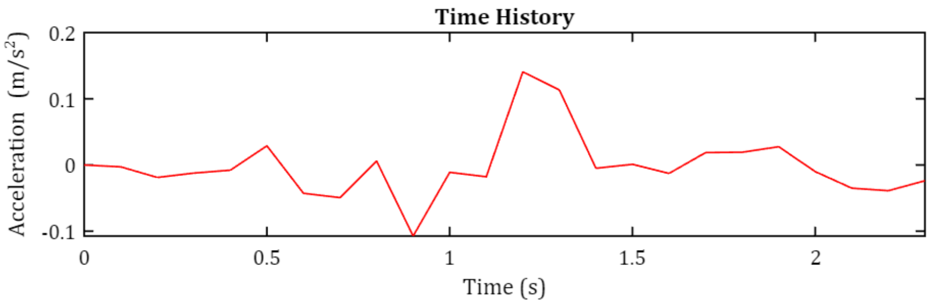

(a)

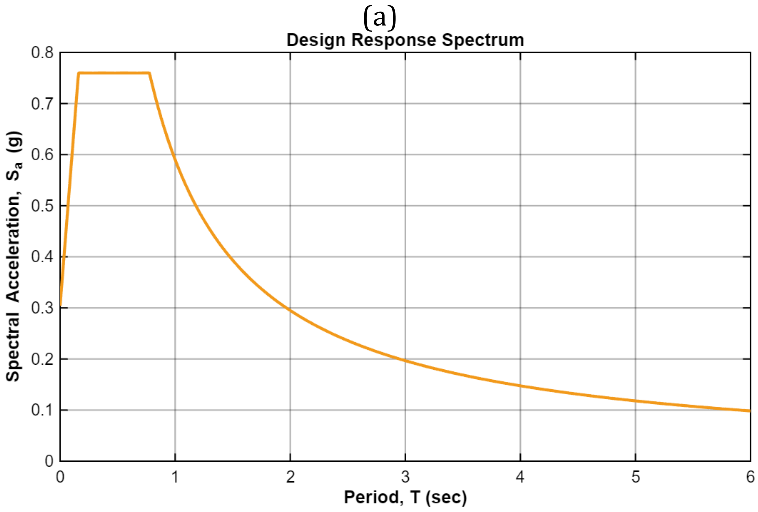

(b)

Fig. 5. Seismic input for time history analysis: (a) acceleration time history record; (b) design response spectrum curve obtained from the Desain Spektra Indonesia application (PU Cipta Karya)

The acceleration time history record used in the dynamic analysis is presented in Figure 5 (a), showing the variation of ground acceleration over time. The corresponding design response spectrum curve, generated from Desain Spektra Indonesia application for the Bogor Regency location, is presented in Figure 5 (b). This spectrum represents the design-level seismic demand for the bridge site with a 7% probability of exceedance in 75 years (return period of approximately 1.000 years) and a medium soil site class (SD). The spectral parameters obtained from the application are PGA = 0,4913g, Ss = 1,0580g, S1 = 0,4815g, SDS = 1,1392g, and SD1 = 0,7311g, as previously presented in Section 2.5.2.

3. Finite Element Analysis Result

3.1 Static Condition Analysis (Service Load)

Static condition analysis aims to evaluate the structural behavior of suspension bridge anchors under static service loading, namely loads that work slowly and constantly, such as the self-weight of the structure, pedestrian live loads, and wind loads under normal conditions. The results of numerical simulations using the three-dimensional finite element method are presented to understand the local response at the anchor connection area in the form of stress contours, elastic strains, and deformations.

3.1.1 Static Stress Distribution

Based on the results of numerical analysis using the finite element method on the suspension bridge anchor connection due to static loading, the overall stress distribution shows a relatively balanced and uniform pattern in various loading directions. The normal stress along the X-axis (S11) and Z-axis (S33) shows a combination of tensile and compressive conditions, with maximum tensile stress ranging from +26,31 MPa to +26,72 MPa and maximum compressive stress ranging from -62,70 MPa to -73,16 MPa. Meanwhile, the shear stress components in the XY (S12), XZ (S13), and YZ (S23) planes show a relatively symmetrical distribution pattern with maximum values ranging from ±19,31 MPa to ±57,05 MPa.

The average stress level reaches approximately 75% of the entire structural domain indicating that the force transfer mechanism in the anchor connection operates effectively without excessive stress concentration at any particular location. This result indicates that the anchor connection can distribute stress efficiently and maintain stable behavior, so that the structure is able to withstand the given service load without significant indication of local failure. The following is shown the static stress output of the anchor connection in (Fig. 6), and a summary of the static stress analysis results in Table 5 below.

Table 5. Recapitulation of static stress analysis results

Stress Type	Notation	Direction	Maximum Stress (MPa)	Minimum Stress (MPa)
Normal Stress	S11	X	+26,31	-62,70
Normal Stress	S33	Z	+26,72	-73,16
Shear Stress	S12	X-Y	+54,28	-57,05
Shear Stress	S13	X-Z	+19,31	-19,46
Shear Stress	S23	Y-Z	+48,61	-53,35

The transfer of forces from the anchor bolt to the surrounding concrete occurs through three primary mechanisms. First, bearing stress develops along the shank of the anchor bolt where it contacts the concrete, transferring compressive and shear forces. Second, friction at the steel-concrete interface contributes to shear resistance, governed by a friction coefficient of 0,3 as defined in the surface-to-surface contact algorithm. Third, the embedment length of 1.200 mm provides sufficient development length to ensure that tensile forces are fully transferred to the concrete through bond and mechanical interlock. Under combined axial, shear, and moment loading, the load path initiates at the top surface of the anchor bolt, travels through the bolt shank, and distributes into the pedestal concrete via bearing and friction at the interface.

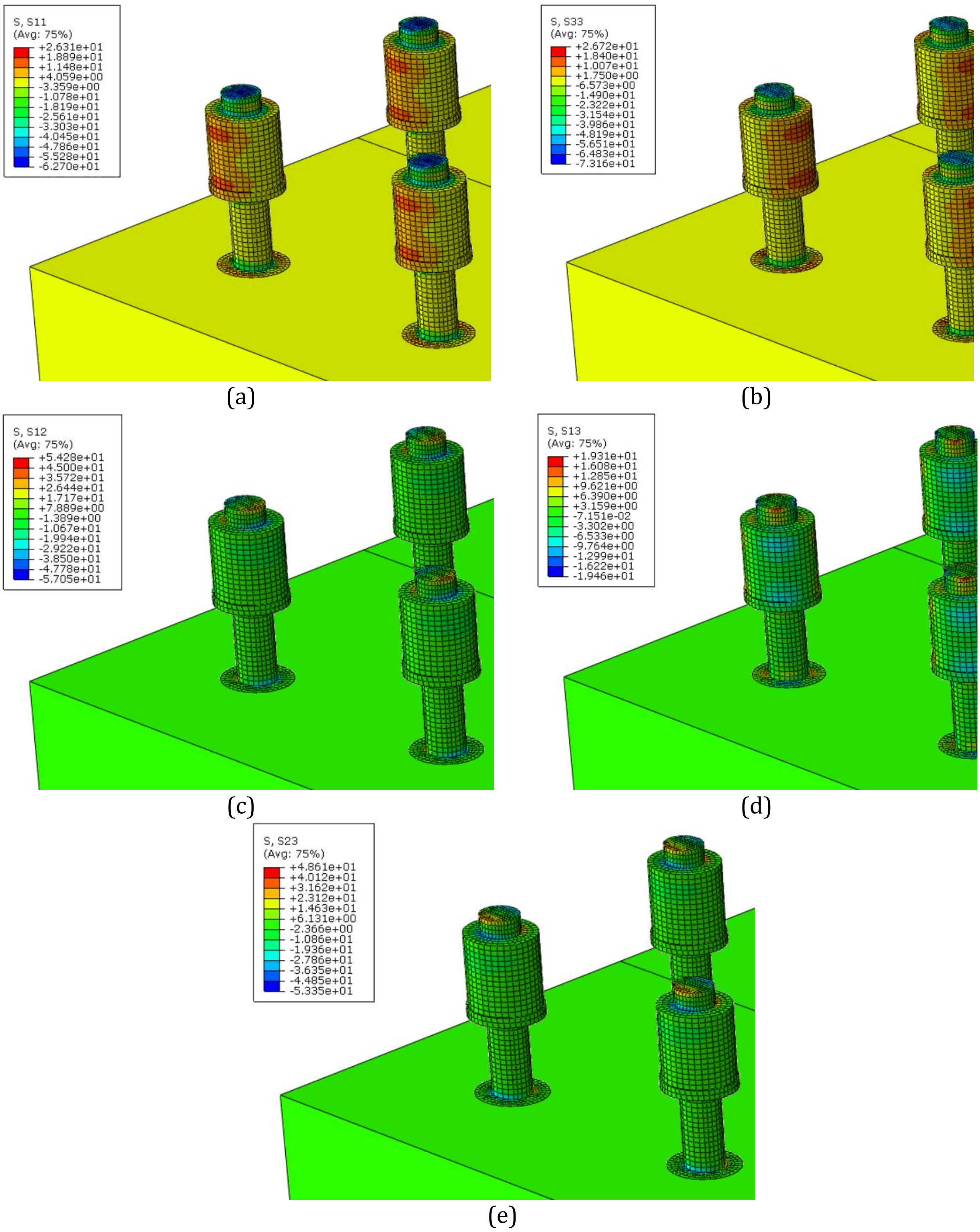

Fig. 6. Stress output of the anchor connection under static loading: (a) S11; (b) S33; (c) S12; (d) S13; (e) S23

This mechanism is reflected in the stress contours presented in Figure 5, where higher stress concentrations are observed at the anchor bolt-concrete interface. In addition to the S11 results, the minimum principal stress was also examined to provide a more comprehensive assessment of the concrete pedestal behavior. While S11 provides information about stress in a specific direction, the minimum principal stress represents the most compressive stress at a point, which is critical for evaluating potential crushing or compressive failure in the concrete pedestal. The minimum principal stress distribution showed a similar pattern to S11 in terms of concentration around the anchor bolt-concrete interface. However, the magnitude of minimum principal stress was generally higher (more compressive) than S11, with localized peaks observed at the bolt-concrete interface due to stress concentration effects. The similarity in distribution patterns confirms the consistency of the results, while the difference in magnitude highlights the importance of considering principal stresses for a complete assessment of concrete performance under combined loading. This reinforces the importance of using a 3D solid element approach (C3D8R) with proper material modeling (Concrete Damage Plasticity) to capture the complex stress states in the anchor connection.

3.1.2 Static Elastic Strain Distribution

Based on the results of numerical analysis using the finite element method on anchor connections due to static loading, in general the strain distribution shows a relatively even pattern throughout the structural components, with higher strain concentrations localized in the meeting area between the anchor bolts and the pedestal concrete due to the transfer of axial, shear, and moment forces.

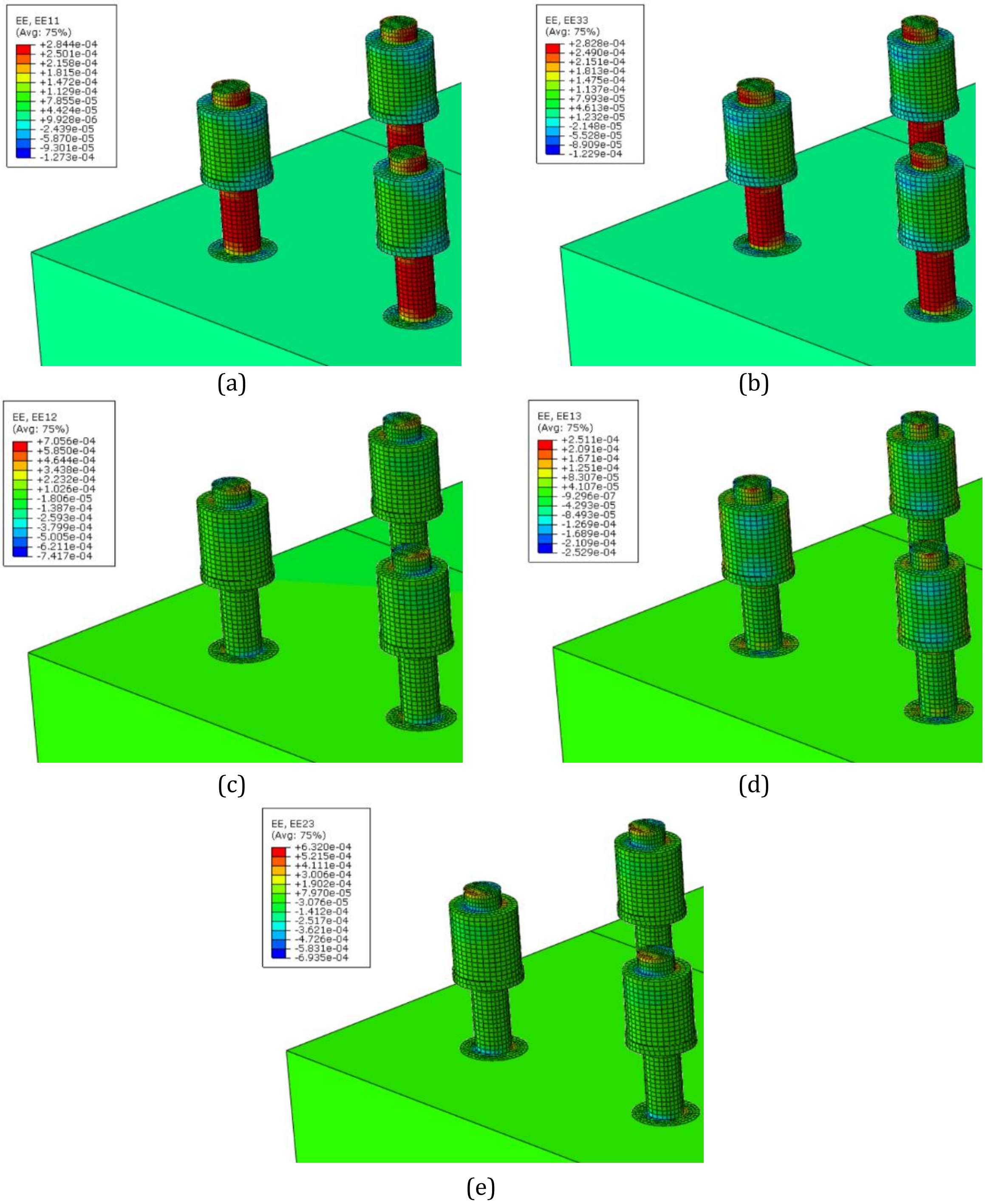

Fig. 7. Elastic Strain output of the anchor connection under static loading: (a) EE11; (b) EE33; (c) EE12; (d) EE13; (e) EE23

The shear strains in the anchor connections show relatively significant values, with maximum strains ranging from ±2,511 x 10^{-4} to ±7,417 x 10^{-4}, which are dominated by the EE12 (XY) and EE23 (YZ) components. This indicates that the shear mechanism plays a dominant role in the behavior of the anchor connection, so that the presence and performance of anchor bolts and anchorage configuration are crucial factors to ensure adequate load transfer capacity. The following shows the output of the elastic strain of the anchor connection under static conditions in (Fig. 7), and a summary of the results of the static elastic strain analysis in Table 6 below.

Table 6. Recapitulation of static elastic strain analysis results

Elastic Strain Type	Notation	Direction	Maximum Strain	Minimum Strain
Normal Elastic Strain	EE11	X	+2,844 x 10^{-4}	-1,273 x 10^{-4}
Normal Elastic Strain	EE33	Z	+2,828 x 10^{-4}	-1,229 x 10^{-4}
Shear Elastic Strain	EE12	X-Y	+7,056 x 10^{-4}	-7,417 x 10^{-4}
Shear Elastic Strain	EE13	X-Z	+2,511 x 10^{-4}	-2,529 x 10^{-4}
Shear Elastic Strain	EE23	Y-Z	+6,320 x 10^{-4}	-6,935 x 10^{-4}

3.1.3 Static Displacement

Based on the numerical results of anchor connections using the finite element method due to static loading, the structural displacement response shows a deformation pattern that is consistent with the working mechanism of suspension bridge anchor connections. The distribution of displacements in the X-axis (U1) and Z-axis (U3) directions is relatively symmetrical with maximum values between ±0,16 mm to ±0,15 mm, while the dominant displacement occurs in the Y-axis (U2) direction with a maximum value of -3,043 x 10^{-1} mm, indicating the main loading direction and lateral response of the structure.

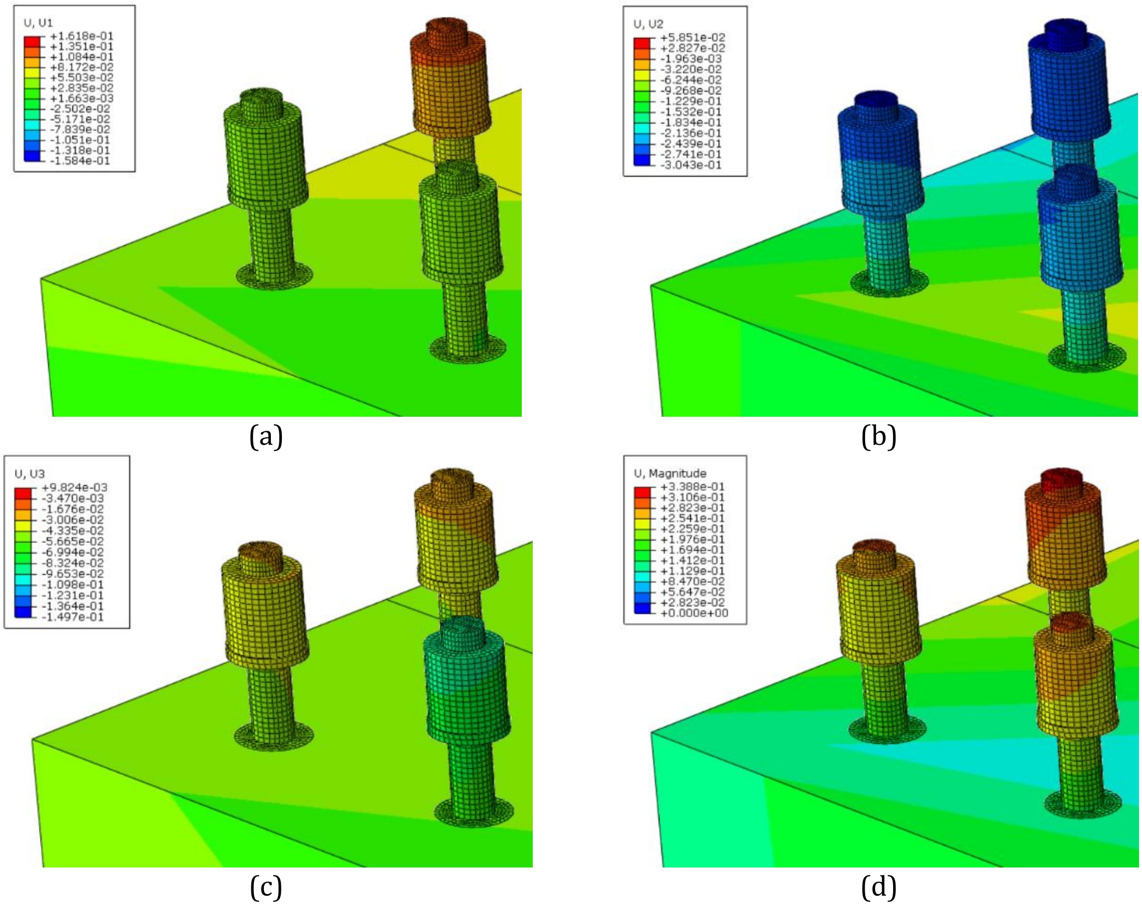

(a) (b)

(c) (d)

Fig. 8. Displacement output of the anchor connection under static loading: (a) U1; (b) U2; (c) U3; (d) UMag

The total displacement pattern (UMag) shows a gradient from the joint core to the edge of the base plate, not toward the column. This condition indicates that the force transfer mechanism at the joint is still effective, with controlled deformation concentration at the elements planned to deform, so that the overall structural response remains in a stable condition under the static load acting on the joint. The following shows the output of the anchor joint deformation under static conditions in (Fig. 8), and a summary of the results of the static deformation analysis in Table 7 below.

Table 7. Recapitulation of static displacement analysis results

Displacement Component	Notation	Direction	Maximum Displacement (mm)	Minimum Displacement (mm)
X-Displacement	U1	X	$+1{,}618 \times 10^{-1}$	$-1{,}584 \times 10^{-1}$
Y-Displacement	U2	Y	$+5{,}851 \times 10^{-2}$	$-3{,}043 \times 10^{-1}$
Z-Displacement	U3	Z	$+9{,}824 \times 10^{-3}$	$-1{,}497 \times 10^{-1}$
Resultant Displacement	UMag	total	$+3{,}388 \times 10^{-1}$	0

The following shows a graph of the analysis results using ABAQUS/CAE V6.14, namely the relationship between displacement and time under static loading conditions.

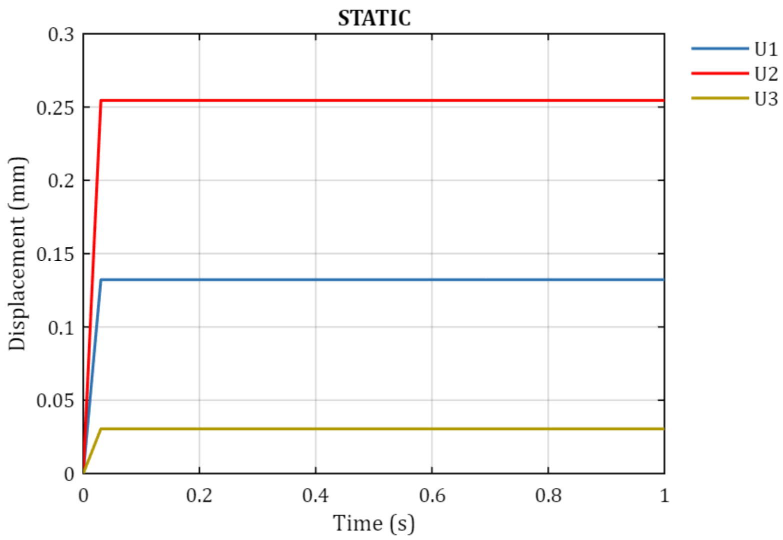

Fig. 9. Displacement versus time graph under static loading conditions, showing the progressive deformation of the anchor connection as the static load was applied incrementally

3.2 Dynamic Condition Analysis (Seismic Load)

The dynamic condition analysis aims to evaluate the response of the suspension bridge anchor structure under earthquake loading modeled using time history analysis. The main objective of this analysis is to understand the dynamic behavior of the anchor system in response to transient and irregular ground motions, as well as to identify the distribution of stress, elastic strain, and maximum deformation that occurs during the earthquake duration.

3.2.1 Dynamic Stress Distribution

Based on the results of numerical analysis using the finite element method on anchor connections due to earthquake dynamic loading with time history analysis, in general the stress distribution shows a relatively balanced and even pattern in various loading directions. The normal stress in the X-axis (S11) and Z-axis (S33) directions shows a combination of tensile and compressive conditions, with maximum tensile stress between +18,71 MPa to +18,96 MPa and maximum compressive stress between -44,50 MPa to -51,98 MPa which occurs at time t = 2,4 seconds.

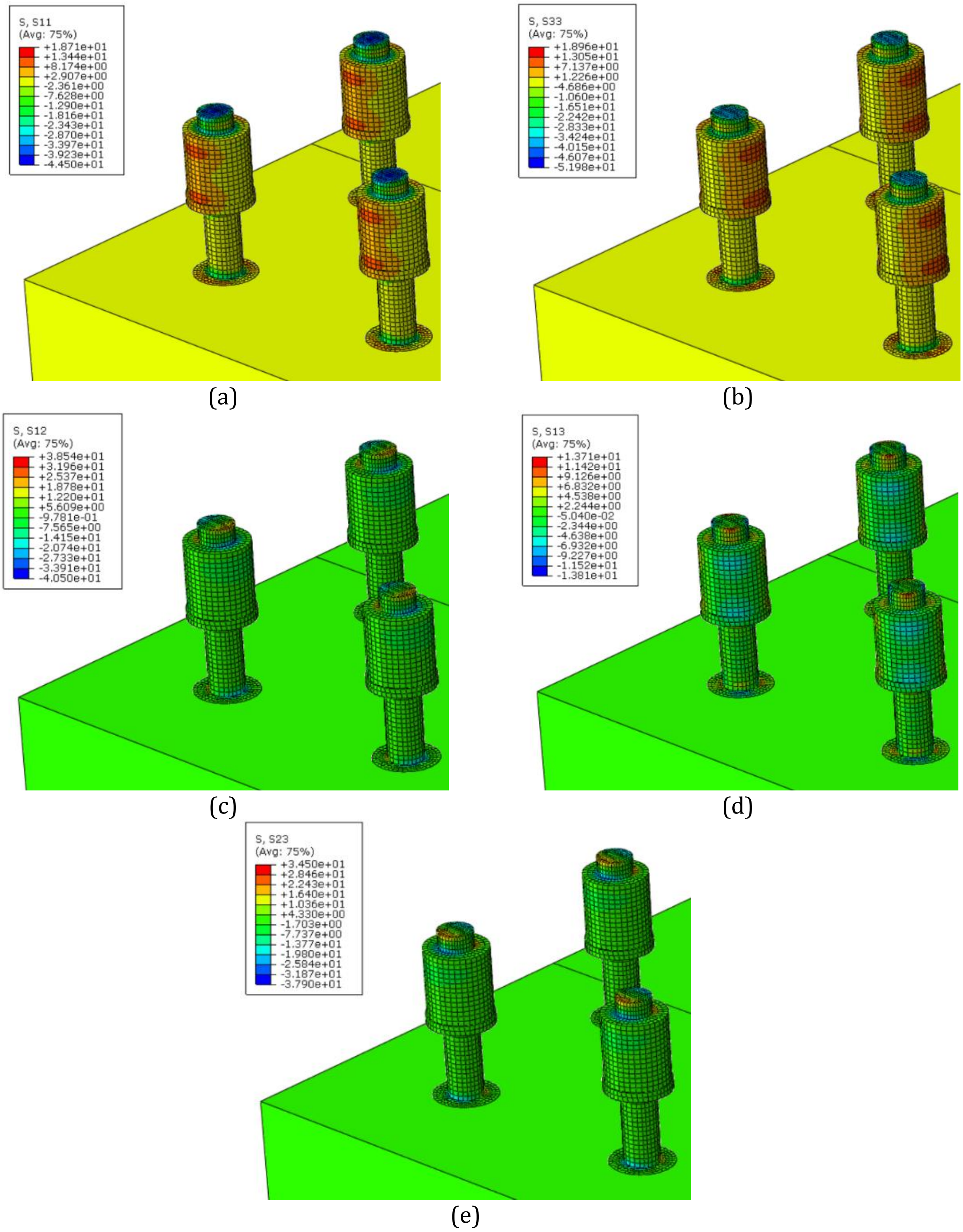

Fig. 10. Stress output of the anchor connection under dynamic loading:
(a) S11; (b) S33; (c) S12; (d) S13; (e) S23

Table 8. Recapitulation of dynamic stress analysis results

Stress Type	Notation	Direction	Maximum Stress (MPa)	Minimum Stress (MPa)
Normal Stress	S11	X	+18,71	-44,50
Normal Stress	S33	Z	+18,96	-51,98
Shear Stress	S12	X-Y	+38,54	-40,50
Shear Stress	S13	X-Z	+13,71	-13,81
Shear Stress	S23	Y-Z	+34,50	-37,90

Meanwhile, the shear stress components in the XY (S12), XZ (S13), and YZ (S23) planes show a relatively symmetrical distribution pattern with maximum values ranging from ±13,71 MPa to ±40,50 MPa. The average stress value of approximately 75% of the entire structural domain indicates that the force transfer mechanism in the interior, exterior, and corner anchor connections operates effectively without excessive stress concentration at certain locations. The following shows the output of the dynamic condition anchor connection stress in (Fig. 10), and a summary of the results of the dynamic condition stress analysis in Table 8 below.

3.2.2 Dynamic Elastic Strain Distribution

Based on the results of numerical analysis using the finite element method on anchor connections due to dynamic earthquake loading, in general the strain distribution shows a relatively even pattern throughout the structural components, with higher strain concentrations localized in the junction area between the base plate and anchor bolts due to the transfer of axial, shear, and moment forces. The normal strains of the X-axis (EE11) and Z-axis (EE33) show a combination of tensile and compressive conditions, with maximum tensile strains between +2,006 x 10^{-4} to +2,018 x 10^{-4} and maximum compressive strains between -8,725 x 10^{-5} to -9,032 x 10^{-5} occurring at time t = 2,4 seconds. The shear strains in the three types of joints show relatively significant values, with maximum strains ranging from ±1,783 x 10^{-4} to ±5,265 x 10^{-4}, which are dominated by the EE12 (XY) and EE23 (YZ) components.

Table 9. Recapitulation of dynamic elastic strain analysis results

Elastic Strain Type	Notation	Direction	Maximum Strain	Minimum Strain
Normal Elastic Strain	EE11	X	+2,018 x 10^{-4}	-9,032 x 10^{-5}
Normal Elastic Strain	EE33	Z	+2,006 x 10^{-4}	-8,725 x 10^{-5}
Shear Elastic Strain	EE12	X-Y	+5,011 x 10^{-4}	-5,265 x 10^{-4}
Shear Elastic Strain	EE13	X-Z	+1,783 x 10^{-4}	-1,796 x 10^{-4}
Shear Elastic Strain	EE23	Y-Z	+4,485 x 10^{-4}	-4,928 x 10^{-4}

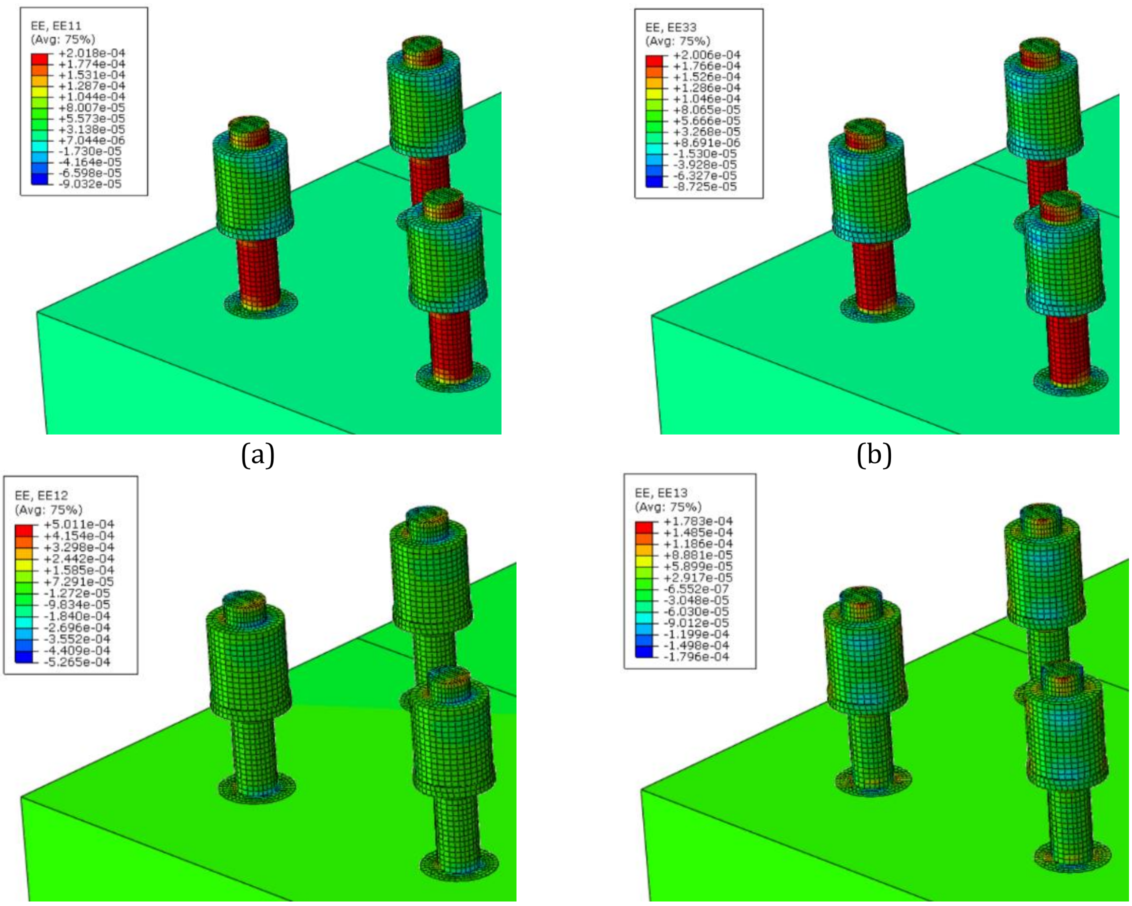

(c) (d)

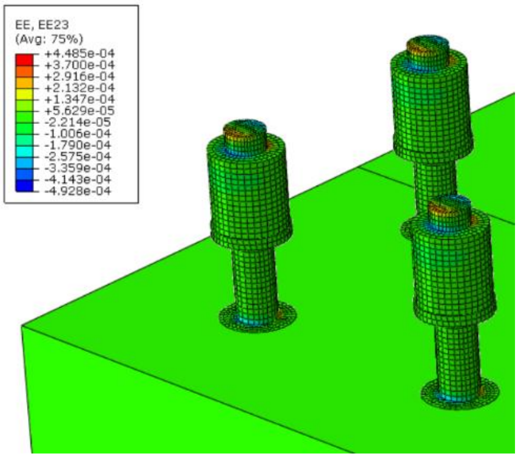

(e)

Fig. 11. Elastic strain output of the anchor connection under dynamic loading: (a) EE11; (b) EE33; (c) EE12; (d) EE13; (e) EE23

This distribution pattern indicates that the deformation mechanism of the connection is influenced by the interaction of normal and shear strains, with a tendency for tensile strains to increase in the critical zone of the connection as the loading level increases, so that the presence and performance of anchor bolts and anchorage configuration are crucial factors to ensure adequate ductility, energy dissipation capacity, and connection performance in accordance with the principles of earthquake-resistant structural design. The following shows the elastic strain output of the dynamic condition anchor connection in (Fig. 11), and a summary of the results of the dynamic condition elastic strain analysis in Table 9 below.

3.2.3 Dynamic Displacement

Based on the numerical results of anchor connections using the finite element method due to earthquake dynamic loading, the structural displacement response shows a deformation pattern that is consistent with the working mechanism of the anchor connection. The distribution of displacements in the Y-axis (U2) and Z-axis (U3) directions is relatively symmetrical with maximum values between ±0,04 mm to ±0,22 mm, while the dominant displacement occurs in the X-axis (U1) direction with a maximum value of +1,126 x 10^{-1} mm, indicating the main loading direction and lateral response of the structure.

The total displacement pattern (UMag) shows a gradient from the joint core to the edge of the base plate, with a maximum value of 2,395 x 10^{-1} mm. This condition indicates that the force transfer mechanism at the joint is still effective, with controlled deformation concentration at the elements planned to deform, so that the overall structural response remains in a stable condition under cyclic loads acting on the joint. The following shows the deformation output of the anchor joint under dynamic conditions in (Fig. 12), and a summary of the results of the dynamic deformation analysis in Table 10 below.

Table 10. Recapitulation of dynamic displacement analysis results

Displacement Component	Notation	Direction	Maximum Displacement (mm)	Minimum Displacement (mm)
X-Displacement	U1	X	+1,126 x 10^{-1}	-1,104 x 10^{-1}
Y-Displacement	U2	Y	+4,161 x 10^{-2}	-2,162 x 10^{-1}
Z-Displacement	U3	Z	+6,986 x 10^{-3}	-1,040 x 10^{-1}
Resultant Displacement	UMag	total	+2,395 x 10^{-1}	0

The following graph shows the results of the analysis using ABAQUS/CAE V6.14, namely the relationship between force and displacement with time under dynamic earthquake loading conditions with time history analysis. This graph illustrates the hysteresis response of the anchor system which represents the force-displacement relationship at a specific observation point during the duration of the earthquake loading.

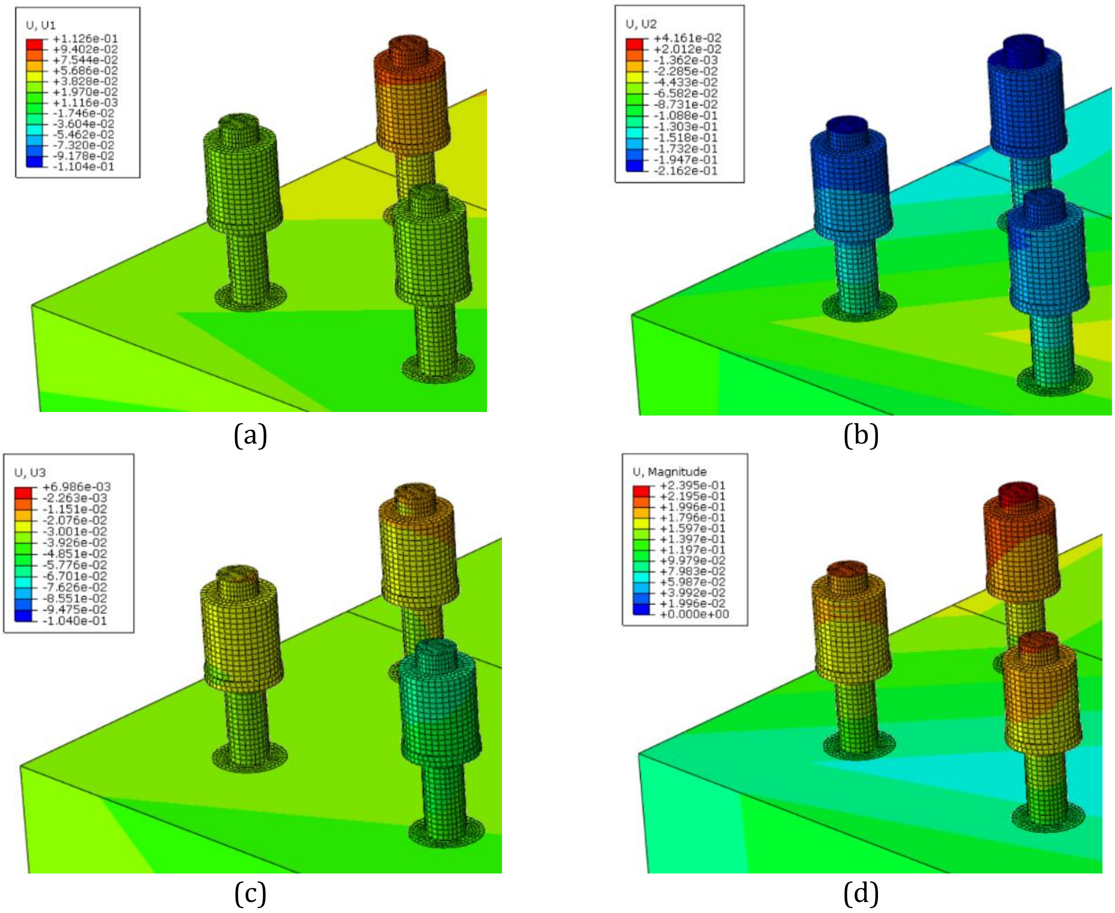

Fig. 12. Displacement output of the anchor connection under static loading: (a) U1; (b) U2; (c) U3; (d) UMag

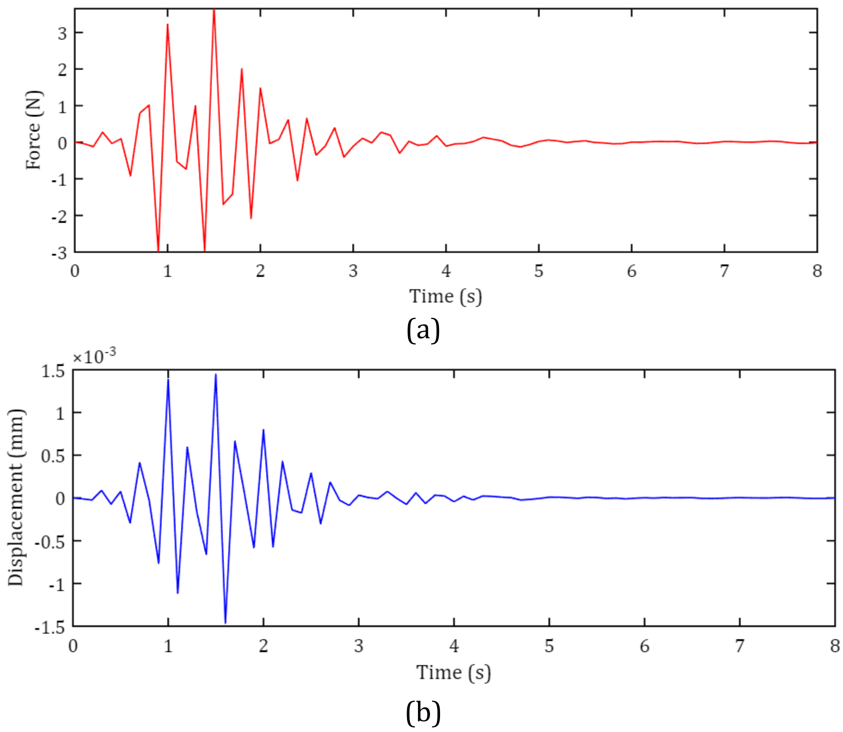

Fig. 13. Time history response of the anchor connection under seismic loading: (a) force versus time; (b) displacement versus time

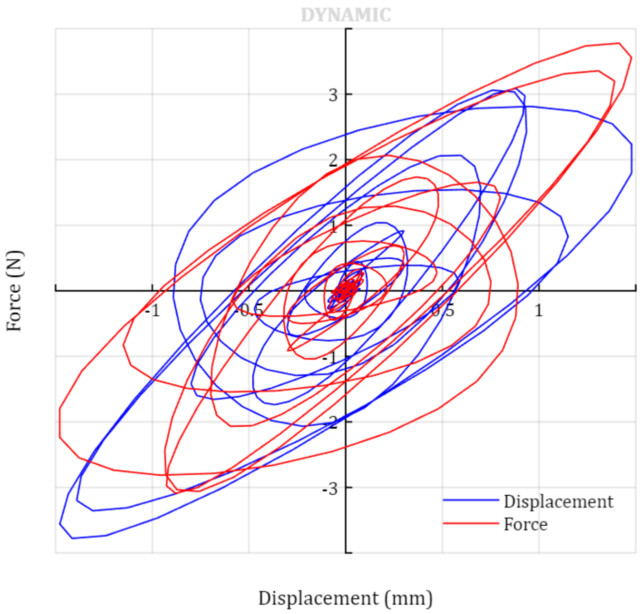

Fig. 14. Force-displacement hysteresis curve under seismic loading. Red curve indicates loading path; blue curve indicates unloading path

3.3 Design Verification and Performance Evaluation

The factored load combination used in this verification is 1,2D + 1,6L + 0,5W (static service condition), as previously discussed in Section 2.3.2. This combination produced the maximum reaction forces at the anchor connection, resulting in an axial force of Pu = 17.329 kN, a bending moment of Mu = 9.667 kNm, and a shear force of Vu = -7.675 kN. These values are used as the basis for the demand-capacity ratio (DCR) calculations in the following sub-sections.

3.3.1 Verification of Anchor Bolt Tensile Capacity

Based on manual calculations, the tensile force on the anchor bolt (T_u) that occurs due to the factored load combination is 10.500 kN. With the number of bolts on the tensile side as many as 34 pieces, the maximum tensile force of one anchor bolt (T_{rod}) is 308,87 kN. The cross-sectional area of the anchor bolt threaded area (A_{se}) is calculated as 883 mm², so the nominal tensile strength of the anchor bolt $(N_{sa}) = A_{se} \times f_u = 883\ \text{mm}^2 \times 830\ \text{MPa} = 732.677\ \text{N} \approx 732{,}68\ \text{kN}$. With a tensile strength reduction factor (ϕ_t) = 0,75, the tensile resistance of the anchor bolt is $(\phi_t N_{sa}) = 0{,}75 \times 732{,}68 = 549{,}51\ \text{kN}$. The verification results show that the maximum tensile force of one anchor bolt (308,87 kN) is smaller than the tensile resistance of the anchor bolt (549,51 kN), so that the anchor connection is declared SAFE against tensile loads.

3.3.2 Verification of Anchor Bolt Shear Capacity

The shear force on the anchor bolt (V_{u1}) that occurs due to the factored loading combination is -112,877 N. The cross-sectional area of the anchor bolt in the unthreaded area (A_{bolt}) = 1.018 mm². With the number of shear planes (m) = 1 and the thread influence factor on the shear plane (r_1) = 0,4, the nominal shear resistance $(V_n) = r_1 \times m \times A_{bolt} \times f_u = 0{,}4 \times 1 \times 1.018 \times 830 = 337.976\ \text{N} \approx 337{,}98\ \text{kN}$. With the shear strength reduction factor (ϕ_f) = 0,75, the shear resistance of the bolt anchor $(\phi_f V_n) = 0{,}75 \times 337{,}98\ \text{kN} = 253{,}49\ \text{kN}$. The verification results show that the shear force on the bolt anchor (112.88 kN) is smaller than the shear resistance of the bolt anchor (253.49 N), so that the anchor connection is declared SAFE against shear loads. The combined tension-shear interaction check is explicitly presented in Section 3.3.3, which confirms that the anchor connection satisfies the AISC 360-16 criteria with a demand-capacity ratio (DCR) of 0,65.

3.3.3 Verification of Shear and Tensile Force Combinations

Verification of the combination of shear and tensile forces was carried out based on the provisions of AISC 360-16. The nominal tensile stress of the anchor$(F_{nt}) = 0{,}75 \times f_u = 0{,}75 \times 830 = 622{,}50\ \text{MPa}$. The nominal shear stress of the anchor $(F_{nv}) = 0{,}45 \times f_u = 0{,}45 \times 830 =$

373,50 MPa. The tensile stress of the anchor due to the combination of shear and tension was calculated at 466,88 MPa. The stress that occurs in the anchor bolt from the FEM analysis (303,44 MPa) is smaller than the tensile stress of the anchor due to the combination of shear and tension (466,88 MPa), so that the anchor connection is declared SAFE against the combination of tensile and shear loads.

3.3.3 Verify Anchorage Length

The anchor length used (La) = 1.200 mm. The minimum anchor length required (L_{min}) is calculated based on the equation:

$$L_{min} = \frac{f_y}{\left(4 \times \sqrt{f'c}\right) \times d} = \frac{660}{\left(4 \times \sqrt{30}\right) \times 36} = 836\, mm \tag{3}$$

The verification results show that the anchor length used (1.200 mm) is greater than the minimum anchor length required (836 mm), so that the anchor connection is declared SAFE against the anchorage length requirements.

3.3.4 Demand-Capacity Ratio

The demand-capacity ratio (DCR) for critical components of anchor connections is calculated as follows:

Table 11. Ratio demand-capacity (DCR)

Component	Demand	Capacity	DCR	Status
Anchor bolt tension	308.867 N	549.508 N	0,56	Safe
Anchor bolt shear	112.877 N	253.451 N	0,45	Safe
Tension-shear combination	303,44 MPa	466,88 MPa	0,65	Safe
Embedment length	836 mm	1.200 mm	0,70	Safe

All DCR ratios are below 1.0, confirming that the anchor connection design meets the safety criteria based on applicable AISC standards.

4. Conclusion

Based on the results of numerical analysis using the finite element method on the anchor connection of the pedestrian suspension bridge due to service and seismic loads, it is concluded that the integration of CSi Bridge v25 and ABAQUS/CAE V6.14 software proved effective in representing the behavior of anchor connections in macro and micro, where macro modeling succeeded in representing the global response of the structure accurately while micro modeling was able to identify the distribution of stress, elastic strain, and local deformation patterns with high detail. Under static loading conditions, the anchor connection remains within the elastic limit with a maximum stress recorded at +26,72 MPa in tensile normal stress, -73,16 MPa in compressive normal stress, and +54,28 MPa in shear stress, and a maximum deformation of 3,388 x 10^{-1} mm which was still far below the design tolerance limit (L/200 = 1.375 mm). Under dynamic loading conditions, the response of the anchor structure shows significant stress and deformation fluctuations with the maximum stress recorded in the normal compressive stress component S33 of -51,98 MPa and shear stress S12 of +38,54 MPa, as well as a maximum deformation of 2,395 x 10^{-1} mm, where these values are still far below the permissible anchor material capacity (bolt yield stress of 660 MPa). Design verification based on AISC 360-16 confirms that the anchor connection meets all safety criteria with a demand-capacity ratio for anchor bolt tension of 0,56, anchor bolt shear of 0,45, combined tension-shear of 0,65, and anchorage length of 0,70, where all DCR ratios are below 1,0 so that the anchor connection is stated and reliable in supporting the performance of suspension bridges in seismic areas. Despite the comprehensive numerical analysis presented in this study, experimental validation is necessary to fully confirm the accuracy of the simulated anchor behavior. Future research should include full-scale laboratory testing, such as pull-out tests and cyclic loading tests, to validate the numerical predictions and to investigate the inelastic response of anchor connections under extreme seismic demands. The bilinear elastoplastic model adopted for the anchor bolts assumes perfect plasticity without strain hardening. While this simplification is acceptable for the present analysis because the anchor remained within the elastic range (maximum stress from FEM analysis 303,44 MPa < yield stress 660 MPa), future studies involving larger inelastic deformations should employ more advanced constitutive models, such as the kinematic hardening model or Chaboche cyclic plasticity model, to capture strain hardening and cyclic degradation effects under repeated seismic loading. The current analysis assumed fully fixed boundary conditions at the pedestal concrete base, neglecting foundation flexibility and soil-structure interaction (SSI). While this simplification is conservative for anchor connection force demands (representing an upper bound), future studies should incorporate SSI effects, especially for bridges located on soft soil deposits where foundation compliance can significantly alter the dynamic response, natural frequencies, and energy dissipation characteristics of the overall bridge system.

References

[1] Chen YJ, Wang S, Zhong JW, Lian F. Study on static analytical method of multi-tower self-anchored suspension bridge. Appl Sci. 2022;12(17):8499. https://doi.org/10.3390/app12178499

[2] Widyaningsih E. Evaluasi keandalan jembatan gantung pejalan kaki dengan variasi letak dan jenis beban lalu lintas. J Teknol Ramah Lingkung. 2020;4(2):71-81. https://doi.org/10.26760/jrh.v4i2.24-34

[3] Yao J, Zhao R, Zhang N, Yang D. Vibration isolation effect study of in-filled trench barriers to train-induced environmental vibrations. Soil Dyn Earthq Eng. 2019;125:105741. https://doi.org/10.1016/j.soildyn.2019.105741

[4] Lignola GP, Bilotta A, Ceroni F. Assessment of the effect of FRCM materials on the behaviour of masonry walls by means of FE models. Eng Struct. 2019;184:145-157. https://doi.org/10.1016/j.engstruct.2019.01.035

[5] Li D, Uy B, Wang J, Song Y. Behaviour and design of high-strength Grade 12.9 bolts under combined tension and shear. J Constr Steel Res. 2020;174:106292. https://doi.org/10.1016/j.jcsr.2020.106305

[6] Aljabar NJ, Zhao XL, Al-Mahaidi R, Ghafoori E, Motovalli M, Koay YC. Experimental investigation on the CFRP strengthening efficiency of steel plates with inclined cracks under fatigue loading. Eng Struct. 2018;172:877-890. https://doi.org/10.1016/j.engstruct.2018.06.074

[7] American Institute of Steel Construction (AISC). Seismic Provisions for Structural Steel Buildings (ANSI/AISC 341-16). Chicago: AISC; 2020.

[8] Tashakori J, Razzaghi J, Ansari S. Reassessment of current design criteria of plastic hinges in shear links. J Constr Steel Res. 2019;158:350-365. https://doi.org/10.1016/j.jcsr.2019.04.006

[9] Torres-Rodas P, Medalla M, Zareian F, Lopez-Garcia D. Cyclic behavior and design methodology of exposed base plates with extended anchor bolts. Eng Struct. 2022;260:114235. https://doi.org/10.1016/j.engstruct.2022.114235

[10] Wang Z, Xian G. A novel compound cone anchorage system for twisted CFRP rods cables: Experimental investigation and FE analysis. Constr Build Mater. 2025;466:140137. https://doi.org/10.1016/j.conbuildmat.2025.140137

[11] Kappos AJ, Saiidi MS, Aydinoglu MN, Isakovic T. Seismic Design and Assessment of Bridges. Vol. 21. New York: Springer; 2012. https://doi.org/10.1007/978-94-007-3943-7

[12] Erbaş Y, Ghoroubi R, Mercimek Ö, Anıl Ö, Karaalp A. Experimental and numerical investigation of impact behaviour of anchored CFRP-to-concrete bonding interface. Theor Appl Fract Mech. 2024;133:104603. https://doi.org/10.1016/j.tafmec.2024.104603

[13] Xie Y, Xiong E, Wang S, Zhang Y, Taciroglu E. Bond behavior of staggered lap and anchored reinforcement in ultra-high performance concrete. J Build Eng. 2025;114:114329. https://doi.org/10.1016/j.jobe.2025.114329

[14] Momenzadeh S, Seker O, Faytarouni M, Shen J. Seismic performance of all-steel buckling-controlled braces with various cross-sections. J Constr Steel Res. 2017;139:44-61. https://doi.org/10.1016/j.jcsr.2017.09.003

[15] Kusbiantoro A, Kusumawardani R, Nugroho U, Hanif N, Azizah KP. Performa penggunaan rubber isolator pada jembatan girder beton. J Inov Konstr. 2023;2(1):40-47. https://doi.org/10.56911/jik.v2i1.82

[16] Chen CC, Wu WH, Kusbiantoro A, Lai G. Necessity investigation of tie-down devices for single-pylon cable-stayed bridges to resist near-fault earthquakes with finite element models updated by vibration measurements. Struct Infrastruct Eng. 2025;21(4):563-578. https://doi.org/10.1080/15732479.2023.2225053

[17] Wu WH, Chen CC, Kusbiantoro A, Lai G. Finite element model of a cable-stayed bridge updated with vibration measurements and its application to investigate the variation of modal frequencies in

monitoring. Struct Infrastruct Eng. 2024;20(5):760-770. https://doi.org/10.1080/15732479.2022.2132517
[18] Petersen ØW, Øiseth O. Finite element model updating of a long span suspension bridge. In: Proceedings of the International Conference on Earthquake Engineering and Structural Dynamics; 2017 Jun. https://doi.org/10.1007/978-3-319-78187-7_25
[19] Kusumawardani R, Hanif MU, Kusbiantoro A, Azizah KP, Nugroho U, Suwandi S. Structural health monitoring by identification dynamic properties and load rating factor at multi-span prestressed concrete girder bridge. Aceh Int J Sci Technol. 2024;12(3):419-432. https://doi.org/10.13170/aijst.12.3.34451
[20] Kusbiantoro A, Kusumawardani R, Hanif MU, Azizah KP, Nugroho U, Suwandi S. Assessment of dynamic properties and finite element model on single-span concrete girder bridge. Int J Eng Trans B Appl. 2026;39(3):727-738. https://doi.org/10.5829/ije.2026.39.03c.13
[21] Kim W, Lee JH. An improved explicit time integration method for linear and nonlinear structural dynamics. Comput Struct. 2018;206:42-53. https://doi.org/10.1016/j.compstruc.2018.06.005
[22] Hasan H, Abdul Rahman A. Finite element analysis of reinforced concrete bridge pier subjected to seismic loading. Am J Sci Ind Res. 2012;3(2):94-98. https://doi.org/10.5251/ajsir.2012.3.2.94.98
[23] Bonfigli MF, Materazzi AL, Breccolotti M. Influence of spatial correlation of core strength measurements on the assessment of in situ concrete strength. Struct Saf. 2017;68:43-53. https://doi.org/10.1016/j.strusafe.2017.05.005
[24] Massone LM, Melo F. General solution for shear strength estimate of RC elements based on panel response. Eng Struct. 2018;172:701-711. https://doi.org/10.1016/j.engstruct.2018.06.038
[25] Parks JE, Pantelides CP, Ibarra L, Sanders DH. Stretch length anchor bolts under combined tension and shear. ACI Struct J. 2019;115(5):1317-1328. https://doi.org/10.14359/51702236
[26] Xu C, Gu Y, Peng S. Experimental research on anchoring behavior of chemical anchor bolt under repeated loading. IOP Conf Ser Mater Sci Eng. 2020;774(1):012134. https://doi.org/10.1088/1757-899X/774/1/012134
[27] Soules JG, Bachman R, Silva J. Chile Earthquake of 2010: Assessment of Industrial Facilities Around Concepción. 1st ed. Reston (VA): American Society of Civil Engineers; 2016. https://doi.org/10.1061/9780784413647
[28] Kawashima K. Seismic design and retrofit of bridges. Bull N Z Soc Earthq Eng. 2000;33(3):265-285. https://doi.org/10.5459/bnzsee.33.3.265-285
[29] American Association of State Highway and Transportation Officials (AASHTO). AASHTO LRFD Bridge Design Specifications. Customary U.S. Units. Washington (DC): AASHTO; 2012.
[30] American Concrete Institute (ACI). Building Code Requirements for Structural Concrete (ACI 318-19). Farmington Hills (MI): ACI; 2019.
[31] Trautner CA, Hutchinson TC. Parametric finite-element modeling for exposed steel moment frame column baseplate connections subjected to lateral loads. J Struct Eng. 2018;144(6):04018042. https://doi.org/10.1061/(ASCE)ST.1943-541X.0001990
[32] Pan WH, Tao MX, Nie JG. Fiber beam-column element model considering reinforcement anchorage slip in the footing. Bull Earthq Eng. 2017;15(3):991-1018. https://doi.org/10.1007/s10518-016-9987-3
[33] Jeon SH, Park JH, Ha TW. Seismic design of steel moment-resisting frames with damping systems in accordance with KBC 2016. Appl Sci. 2019;9(11):2317. https://doi.org/10.3390/app9112317
[34] Rahmanian M, Farsadi T, Kurtaran H. Nonlinear flutter of tapered and skewed cantilevered plates with curvilinear fiber paths. J Sound Vib. 2021;500:116021. https://doi.org/10.1016/j.jsv.2
[35] Hanif MU, Ibrahim Z, Ghaedi K, Javanmardi A, Rehman SK. Finite element simulation of damage in RC beams. Structural Engineering and Mechanics. 2018. https://doi.org/10.33736/jcest.883.2018
[36] Faveryan IB, Triwiyono A, Siswosukarto S. Numerical modeling of applied near-surface mounted on reinforcement slab with ABAQUS CAE. J Tek Sipil. 2023;17(2):78-83. https://doi.org/10.24002/jts.v17i2.6183